ARMY RESEARCH LABORATORY

Computed In-Flight Temperature Response of a 120-mm XM797 Gas Generator Training Round Nose Cap

Bernard J. Guidos

ARL-MR-267 October 1995

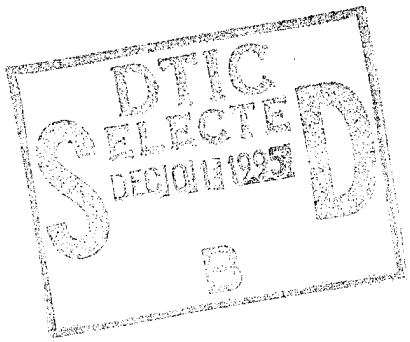

NOTICES

Destroy this report when it is no longer needed. DO NOT return it to the originator.

Additional copies of this report may be obtained from the National Technical Information Service, U.S. Department of Commerce, 5285 Port Royal Road, Springfield, VA 22161.

The findings of this report are not to be construed as an official Department of the Army position, unless so designated by other authorized documents.

The use of trade names or manufacturers' names in this report does not constitute indorsement of any commercial product.

REPORT DOCUMENTATION PAGE

Form Approved
OMB No. 0704-0188

1. AGENCY USE ONLY *(Leave blank)*	2. REPORT DATE	3. REPORT TYPE AND DATES COVERED
		Final, August 1994 - December 1994

4. TITLE AND SUBTITLE

Computed In-flight Temperature Response of a 120-mm XM797 Gas Generator Training Round Nose Cap

5. FUNDING NUMBERS

1L162618AH80

6. AUTHOR(S)

Bernard J. Guidos

7. PERFORMING ORGANIZATION NAME(S) AND ADDRESS(ES)

US Army Research Laboratory
ATTN: AMSRL-WT-PB
Aberdeen Proving Ground, MD 21005-5066

8. PERFORMING ORGANIZATION REPORT NUMBER

9. SPONSORING/MONITORING AGENCY NAMES(S) AND ADDRESS(ES)

10.SPONSORING/MONITORING AGENCY REPORT NUMBER

11. SUPPLEMENTARY NOTES

12a. DISTRIBUTION/AVAILABILITY STATEMENT

Approved for public release; distribution is unlimited.

12b. DISTRIBUTION CODE

13. ABSTRACT *(Maximum 200 words)*

A computational study is presented of the aerothermal response of an XM797 gas generator nosecap. The XM797 nosecap is a critical component in the design of a 120-mm finned kinetic energy (KE) training round projectile. A propellant-filled chamber within the nosecap is designed so that aerodynamic heating ignites the propellant down range, initiating projectile breakup. The objective of this study is to provide the nosecap temperature response, which is necessary to design the chamber geometry. A model for the aerodynamic heat transfer is constructed using a numerical boundary-layer technique. The heat transfer model provides the necessary boundary conditions for a numerical heat conduction analysis, which computes the temperature response throughout the nosecap. Analysis is presented for (1) a 105-mm version of the nosecap for which previous results are available and (2) the 120-mm version of the nosecap currently of interest.

14. SUBJECT TERMS

computational fluid dynamics, supersonic flow, aerodynamic heating, blunt nosetip, heat conduction

15. NUMBER OF PAGES

16. PRICE CODE

17. SECURITY CLASSIFICATION OF REPORT	18. SECURITY CLASSIFICATION OF THIS PAGE	19. SECURITY CLASSIFICATION OF ABSTRACT	20. LIMITATION OF ABSTRACT
UNCLASSIFIED	UNCLASSIFIED	UNCLASSIFIED	SAR

INTENTIONALLY LEFT BLANK.

ACKNOWLEDGMENTS

The author thanks Mr. Brian C. Wong, U.S. Army Armament Research, Development, & Engineering Center (ARDEC), Picatinny Arsenal, New Jersey, for providing necessary drawings, background information, and manuscript review; and Mr. Foster Quevedo, U.S. Army ARDEC, for providing additional background information.

Thanks also to Dr. Gene Cooper, U.S. Army Research Laboratory (ARL), for providing a Bessel function FORTRAN subroutine (which was written, according to Dr. Cooper, by Mr. Alexander S. Elder of the former U.S. Army Ballistic Research Laboratory); Mr. Paul Weinacht, ARL, for technical review of the report; and Mr. Vural Oskay, ARL, for additional reviews.

INTENTIONALLY LEFT BLANK.

TABLE OF CONTENTS

INTENTIONALLY LEFT BLANK.

LIST OF FIGURES

INTENTIONALLY LEFT BLANK.

LIST OF TABLES

INTENTIONALLY LEFT BLANK.

1. INTRODUCTION

This report documents a computational aerothermal analysis of the XM797 gas generator nose cap. The XM797 nose cap is a critical component in the design of a 120-mm finned kinetic energy (KE) training round. The concept is illustrated in Figure 1, taken from Kotar and Quevedo (1983). At launch, the nose cap serves as a forward clamp, holding together multiple sections of the long-rod projectile. A propellant-filled chamber within the nose cap is designed so that aerodynamic heating ignites the propellant at some distance down range, separating all the major projectile components. The training round then breaks apart into high drag pieces that quickly decelerate and impact the ground. Ballistic match is desired between the fielded and training rounds to a range of 3.5 km, with a maximum range less than 12 km.

The objective is to provide the propellant temperature response, which is necessary to design the chamber geometry for training applications. A model for the aerodynamic heat transfer is constructed using a numerical boundary-layer technique. This model provides the necessary boundary conditions for a numerical heat conduction analysis, which computes the temperature response throughout the nose cap. The temperature response at the location of propellant ignition is the key parameter of interest. Once the temperature response is known, the nose cap can be designed for the propellant (and corresponding ignition temperature) of choice.

A 105-mm version of the XM797 nose cap was previously studied (Abbett, Duiven, Laub, and Beck 1981; Kotar and Quevedo 1983; Sturek, Kayser, and Mylin 1983; Sturek, Kayser, Mylin, and Hudgins 1983). For validation, analysis for the 105-mm training round is first presented and compared with the results from Kotar and Quevedo (1983). Next, results are presented for the current 120-mm training round projectile. The modeling approaches for the heat transfer and heat conduction analyses are described, and the relevant modeling assumptions are discussed.

2. CONFIGURATIONS AND FLIGHT CONDITIONS

Figure 2 shows the 105-mm version of the XM797 nose cap. This figure was reproduced from the report by Kotar and Quevedo (1983), in which it is referred to as the "revised design." The nosetip material is given as 18-8ph stainless steel, whose thermal properties are assumed to be the same as 304 stainless steel, shown in Table 1. The propellant chamber is a right-circular cylinder situated along the projectile axis and is sealed with a Teflon®

cup. The nose cap is secured to the multiple-piece rod by a steel piston/aluminum shear pin mechanism designed to fail upon propellant ignition. The in-flight velocity profile (leading to propellant ignition) is assumed to be that of the 105-mm APFSDS-T (armor-piercing, fin-stabilized, discarding sabot with tracer) M833 projectile, as given in Department of the Army Firing Table FT 105-A-3. The launch velocity is 1.49 km/s, and the velocity retardation is approximately 54.0 m/s/km. For the heat conduction computations, the free stream and initial wall temperatures are assumed to be 324 K.

Table 1. Thermal Properties for AIAI-SAE 304 Grade Stainless Steel

Density, ρ (kg/m^3)	7850.0
Conductivity, k (W/m/K)	10.
Specific Heat c_p (J/kg/K)	43.7
Diffusivity, $\alpha=\frac{k}{\rho c_p}$ (m^2/s)	2.9×10^{-5}

Figure 3 shows the 120-mm version of the XM797 nose cap. The basic components of the 120-mm nose cap are the same as those of the 105-mm nose cap. The physical dimensions correspond to those given by the drawing entitled "Nose cap TM-2376," provided by Mr. Brian C. Wong, U.S. Army Armament Research, Development, & Engineering Center, Picatinny Arsenal, New Jersey. The materials are assumed to be the same as those in the 105-mm version. The in-flight velocity profile is taken to be that of the 120-mm APFSDS-T M827 and APFSDS-T DM13 projectiles, whose profiles are almost identical, as given in Department of the Army Firing Table FT 120-D-1. The launch velocity is 1.65 km/s, and the velocity retardation is approximately 74.0 m/s/km. For the heat conduction computations, the free stream and initial wall temperatures are assumed to be equal. Three different cases are considered: 272 K, 294 K, and 324 K, referred to as the "cold," "standard," and "hot" cases, respectively.

The angle of attack is prescribed as 0° for all cases. Atmospheric sea-level free stream pressure and density are assumed. The state of the boundary layer (i.e., laminar, turbulent, and/or transitional) is discussed individually for the 105-mm and 120-mm versions in the results section.

3. MODELING APPROACH

3.1 Surface Heat Transfer Model. Surface heat transfer characteristics were computed using an axisymmetric boundary-layer numerical technique known as the ASCC (ABRES Shape Change Code) reported by Suchsland (1980). The ASCC code uses a mod-

ified Newtonian surface pressure distribution and inviscid flow field approximations to generate boundary-layer edge flow conditions. The ASCC code was used in this study because it generates adiabatic wall temperatures and heat transfer coefficients in 1 or 2 minutes of central processing unit (CPU) time on a typical workstation or mini-computer, as opposed to Navier-Stokes methods, which usually take more CPU time.

Previous work at the U.S. Army Research Laboratory[1] (ARL) included comparison of ASCC and Navier-Stokes results for KE projectile nosetips and published experimental measurements (Guidos and Sturek 1993). The computed laminar heat transfer rates compared well, but the turbulent results showed that the ASCC code underpredicted the heat transfer rates by about 40% at 1.7 km/s, compared to the Navier-Stokes results. For this reason, the turbulent heat transfer rates computed by the ASCC code for this study were increased by 40% before being used in the heat conduction analysis.

The formulation of the heat transfer model follows the procedure outlined by Guidos and Weinacht (1993). Newton's Law of Cooling is applied to form a distribution of heat transfer coefficient, h, at various velocities of interest, i.e.,

$$h = \frac{q}{T_{aw} - T_w} \tag{1}$$

in which T_{aw} is the computed adiabatic wall temperature, q is the computed heat transfer rate, and T_w is wall temperature at which the heat transfer rate is computed. In the study done by Guidos and Weinacht (1993), T_{aw} was held constant over the body surface at each velocity, since the nosetip was ignored in the analysis. In the present study, T_{aw} is computed as a function of axial distance from the nosetip (i.e., stagnation point) at two different velocities bound that of the projectile in flight.

The adiabatic wall temperature, T_{aw}, is represented by a free stream recovery factor, r_f, defined as

$$r_f = \frac{T_{aw} - T_\infty}{T_0 - T_\infty} \tag{2}$$

in which T_∞ and T_0 are the free stream and total temperatures, respectively. The use of r_f serves to normalize the behavior of T_{aw} for different flight velocities.

For the 105-mm case, the heat transfer model is formed using results at velocities 1.49 km/s and 1.27 km/s; for the 120-mm case, the heat transfer model is formed using results at velocities 1.65 km/s and 1.43 km/s. In both cases, the ASCC results are generated assuming a free stream temperature of 294 K. For convenient reference, the total temperatures for each of the velocities of interest is calculated from compressible flow theory (Zucrow and Hoffman 1976) and is given in Table 2.

[1] Formerly the U.S. Army Ballistic Research Laboratory (BRL)

Table 2. Total Temperature for Flight Velocities of Interest, Assuming T_∞=294 K

Velocity (km/s)	Mach Number	T_0(K)
1.65	4.8	1649.
1.49	4.3	1381.
1.43	4.16	1312.
1.27	3.7	1099.

The heat transfer coefficients are held constant with respect to wall temperature and free-stream temperature. In the study of Guidos and Weinacht (1993), it was found that h decreases slightly as T_w increases toward T_{aw}. Thus, the assumption of constant h based on atmospheric wall temperatures will contribute to a slight underprediction of the projectile temperature.

3.2 In-Depth Heat Conduction. The transient in-depth heat conduction analysis was made using the numerical code described by Dwyer (1990); Sturek, Dwyer, and Ferry (1990); Yam (1991); and Sturek (1993). The scheme is a 3-D, time-accurate, implicit, finite volume technique cast in generalized coordinates. For this study, an axisymmetric version of the code was used. The computations were performed using a single processor on a Silicon Graphics Inc. Challenge XL/R4400 computer, with each case requiring approximately 1.5 hours of CPU time. One of the strengths of this code is its fast execution, because of its implicit formulation. Some weaknesses of the code are that its application is limited to single-zone, single-material, constant thermal property cases. The technique has recently been validated for the case of axisymmetric convective heating of an infinite-length rod, for which an analytical solution (Schneider 1955) is available (see the appendix).

The problem setup is shown in Figure 4, and the grid is shown in Figure 5. The cup seal is used as the aft grid boundary and is assumed to form an adiabatic surface perpendicular to the projectile axis. Table 3 shows the thermal properties of Du Pont Teflon®, obtained from a Du Pont Product Information Chart (1995) and Modern Plastics Encyclopedia (1991). The diffusivity is two orders of magnitude less than that of stainless steel, demonstrating the insulative nature of the seal. The adiabatic boundary formed by the seal is then assumed to extend radially outward to the projectile surface.

Conforming to the single-zone, single-material restriction, the propellant chamber is modeled as solid stainless steel. Since the chamber is located in the general area of lowest expected thermal gradients, this simplification is acceptable as a baseline case. But the thermal behavior of the propellant is worth considering in more detail. Table 4 shows approximate thermal

Table 3. Thermal Properties for Du Pont Teflon®

Density, ρ (kg/m^3)	1600.
Conductivity, k (W/m/K)	0.239
Specific Heat c_p (J/kg/K)	1088.
Diffusivity, $\alpha=\frac{k}{\rho c_p}$ (m^2/s)	1.4×10^{-7}

properties of several propellants following Cohen, Beyer, Bilyk and Newberry (1992) and Ward (1974). The properties are quite similar to those of the cup seal, demonstrating that the propellant chamber serves as a good insulator for the rest of the nose cap section. It may be concluded that modeling the propellant chamber as solid stainless steel will contribute to a slight underprediction of the nose cap temperature.

Table 4. Thermal Properties for M9, JA2, M30, and X14 Propellants

Density, ρ (kg/m^3)	1600.
Conductivity, k (W/m/K)	0.234
Specific Heat c_p (J/kg/K)	1465.
Diffusivity, $\alpha=\frac{k}{\rho c_p}$ (m^2/s)	1.0×10^{-7}

In retrospect, an improved prediction could probably be obtained from the single-zone, single-material approach by modeling the chamber wall as adiabatic with respect to the heat flow in the stainless steel. The penalty would be the need to construct an irregular computational grid coincident with the chamber wall, rather than the current grid which is coincident with the projectile axis. An effort is under way to use a newly available multiple zone, multiple material, variable thermal properties heat conduction code.

4. RESULTS

4.1 105-mm XM797 Nose cap. As a means of validating the current modeling approach for a similar problem, analysis was first conducted for the 105-mm version of the XM797 nose cap, for which previous results have been published by Kotar and Quevedo (1983). Few details of the heat transfer and heat conduction modeling, which was conducted by AVCO, are included in the aforementioned report. However, that report does include some additional nosetip transient thermal response predictions that compare favorably with unreferenced arc jet tests, giving a measure of confidence to the free flight results presented there.

In the current approach, the aerodynamic heat transfer parameters are computed using the ASCC code before computing the in-depth heat conduction. Figure 6 shows the computed recovery factors for the 105-mm XM797 nose cap at 1.49 km/s (launch velocity) and 1.27 km/s (uninterrupted velocity at 4-km range). The distribution is shown as a function of axial location, x, normalized by a reference length, l, equal to 25.4 mm (1 inch). The recovery factor as computed by the ASCC code is the same for laminar and turbulent flows. Much experimental data exists showing the recovery factor to differ between laminar and turbulent flows by about 5% (see Guidos & Weinacht [1993] for a more detailed discussion). In the present study, the accuracy of analysis is not compromised because the same recovery factor distribution is used in both the formulation and application of the heat transfer model.

Figures 7 and 8 show the computed 105-mm XM797 heat transfer coefficients used in the present heat conduction analysis. The fully turbulent and fully laminar cases are shown. As previously mentioned, the turbulent heat transfer coefficients computed by the ASCC code were scaled by a factor of 1.4 before being used in the heat conduction analysis. It is assumed that the heat transfer coefficient and adiabatic wall temperature both vary linearly with respect to velocity during the trajectory.

Figure 9 shows the computed temperature response at the location of propellant ignition within the nose cap. Propellant ignition is assumed to occur at the forward outer corner of the propellant chamber. The forward corner of the propellant chamber is located 19.94 mm (0.785 inches) down stream from the stagnation point and 2.51 mm (0.099 inches) off axis, as shown in Figure 2. The present results are shown for both the fully laminar and fully turbulent heating cases. The computed temperature difference between the laminar and turbulent cases is near 150 K at 2 seconds into the flight, indicating large sensitivity of propellant ignition to the state of the boundary layer. Considering that a typical propellant ignition temperature is 500 K or more, it may be concluded that a laminar flow situation will not heat the nose cap sufficiently to ignite the propellant, making a boundary layer trip (i.e. surface knurling) a necessary design component.

Figure 9 also includes the results from Kotar and Quevedo (1983), which differ from the present turbulent results by, at most, only 20 K during the first 4 seconds of flight. The comparison suggests that the previously published results were generated for a fully turbulent flow case.

4.2 120-mm XM797 Nose cap. With the modeling approach validated for the 105-mm version of the XM797 nose cap, results were then generated for the 120-mm version. Figure 10 shows the computed recovery factors for the 120-mm version at 1.65 km/s (launch

velocity) and 1.43 km/s (uninterrupted velocity at 3 km range). As was the case for the 105-mm version, the recovery factors computed by the ASCC code were the same for laminar and turbulent flows.

Figures 11 and 12 show the computed 120-mm XM797 heat transfer coefficients used in the heat conduction analysis. The analysis was done by assuming boundary layer transition to occur over a section of surface knurling (not shown in Figure 3) near the nosetip. The heat transfer coefficient in the transition region, h_{tr}, was generated by combining the fully laminar and fully turbulent distributions using the expression

$$h_{tr} = h_l + \kappa_t(h_t - h_l) \qquad \text{for } x_1 < x < x_2 \tag{3}$$

in which h_l and h_t are the laminar and turbulent heat transfer coefficients, respectively, at a specified x location; x_1 (equal to 2 mm) and x_2 (equal to 10 mm) are the beginning and end, respectively, of transition; and κ_t is the transition intermittency factor. This factor is identically zero for laminar flow and identically one for fully turbulent flow. The assumed form of κ_t in the transition region is that of a 5th order polynomial, as previously used by Guidos, Weinacht, and Dolling (1990). As in the 105-mm case, the turbulent heat transfer coefficients computed by the ASCC code were scaled by a factor of 1.4 before being used in the heat conduction analysis.

Figure 13 shows the computed temperature response at the location of propellant ignition within the nose cap. Once again, propellant ignition is assumed to occur at the forward outer corner of the propellant chamber. The forward corner of the propellant chamber is located 23.62 mm (0.93 inches) down stream from the stagnation point and 2.3 mm (0.0905 inches) off axis, as shown in Figure 3. For a propellant ignition temperature of 500 K, ignition is computed to occur at about 2.1 seconds (3 km range) into flight. The cold, standard, and hot cases are shown to differ by a total of 30 K or less for flight times greater than 2 seconds. This translates into less than 1/3 of a second variation in propellant ignition onset.

Figure 14 shows computed temperature contours within the nose cap at several times during flight for the standard case. The orientation of the contours verifies the contention that the highest chamber temperature (thus ignition) occurs at the forward corner of the chamber.

Figure 15 presents the complete temperature distribution at various times in a form useful for possible design modifications. The temperature distribution is shown as a function of propellant chamber depth, d/l. The chamber depth is measured from the base of the nose cap (refer to Figure 3) and is currently 24.89 mm (0.98 in). Figure 14 depicts the fact that the forward corner of a deeper propellant chamber is closer to the nosetip, and accordingly experiences a higher heating rate. Noting that the time of flight at 3.5 km range

is approximately 2.3 seconds, the depth of the chamber can be varied to correspond to the selected propellant's ignition temperature. Figure 15 shows that for a propellant ignition temperature of 500 K, a 2.54 mm (0.1 inch) increase in chamber depth hastens the ignition time by slightly less than 1/2 second.

5. CONCLUSION

A computational aerothermal analysis of the XM797 gas generator nose cap was presented. The temperature response of the nose cap is a critical component in the design of 105-mm and 120-mm finned KE training round projectiles, which use the XM797 concept. The temperature response within the propellant chamber inside the nose cap is the key parameter of interest.

Analysis was first presented for a 105-mm version of the XM797 nose cap using flight conditions from an M833 projectile. The computed temperature response at the forward corner of the propellant chamber compared favorably with previously published results, validating the present modeling approach.

Analysis for the 120-mm version of the XM797 nose cap was performed using flight conditions from a DM13 projectile. The analysis was done for the boundary-layer transition case, in which the boundary layer is tripped by a section of surface knurling near the nosetip. For a propellant ignition temperature of 500 K, ignition is computed to occur at about 2.1 seconds (3 km range) into the flight. Results for cold, standard, and hot wall cases show relatively minor differences which translate into less than 1/3 second variation in propellant ignition onset. For the current design, a 2.54-mm (0.1-inch) increase in chamber depth hastens the ignition time by approximately 1/2 second.

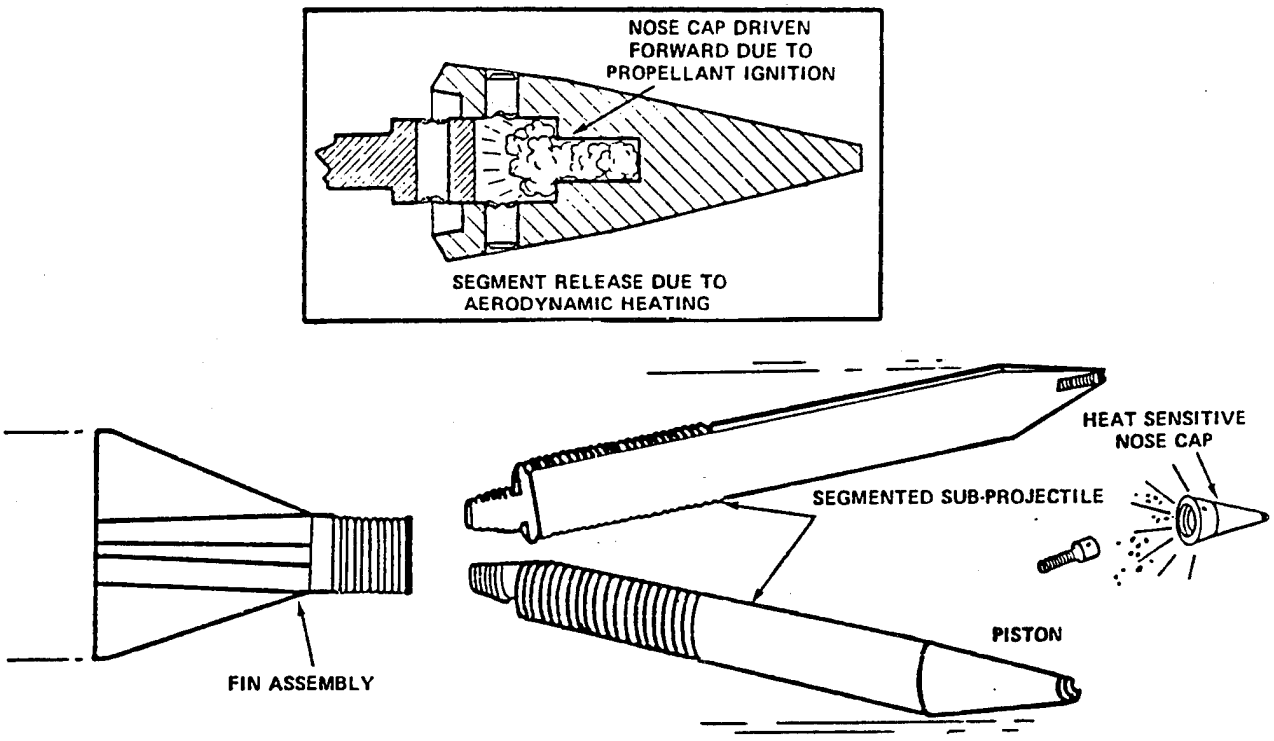

Figure 1. XM797 Gas Generator Nosecap Concept

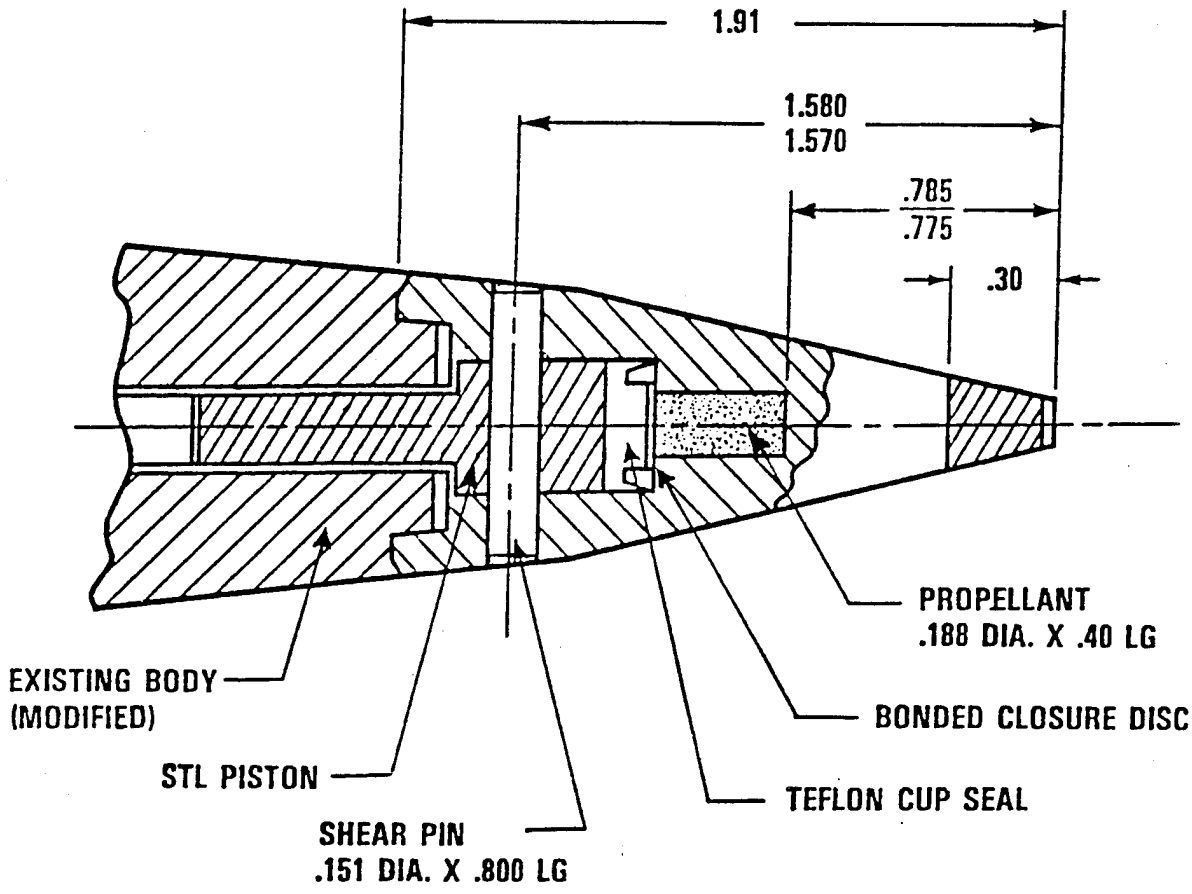

Dimensions in inches

Figure 2. Schematic of 105-mm XM797 Nosecap

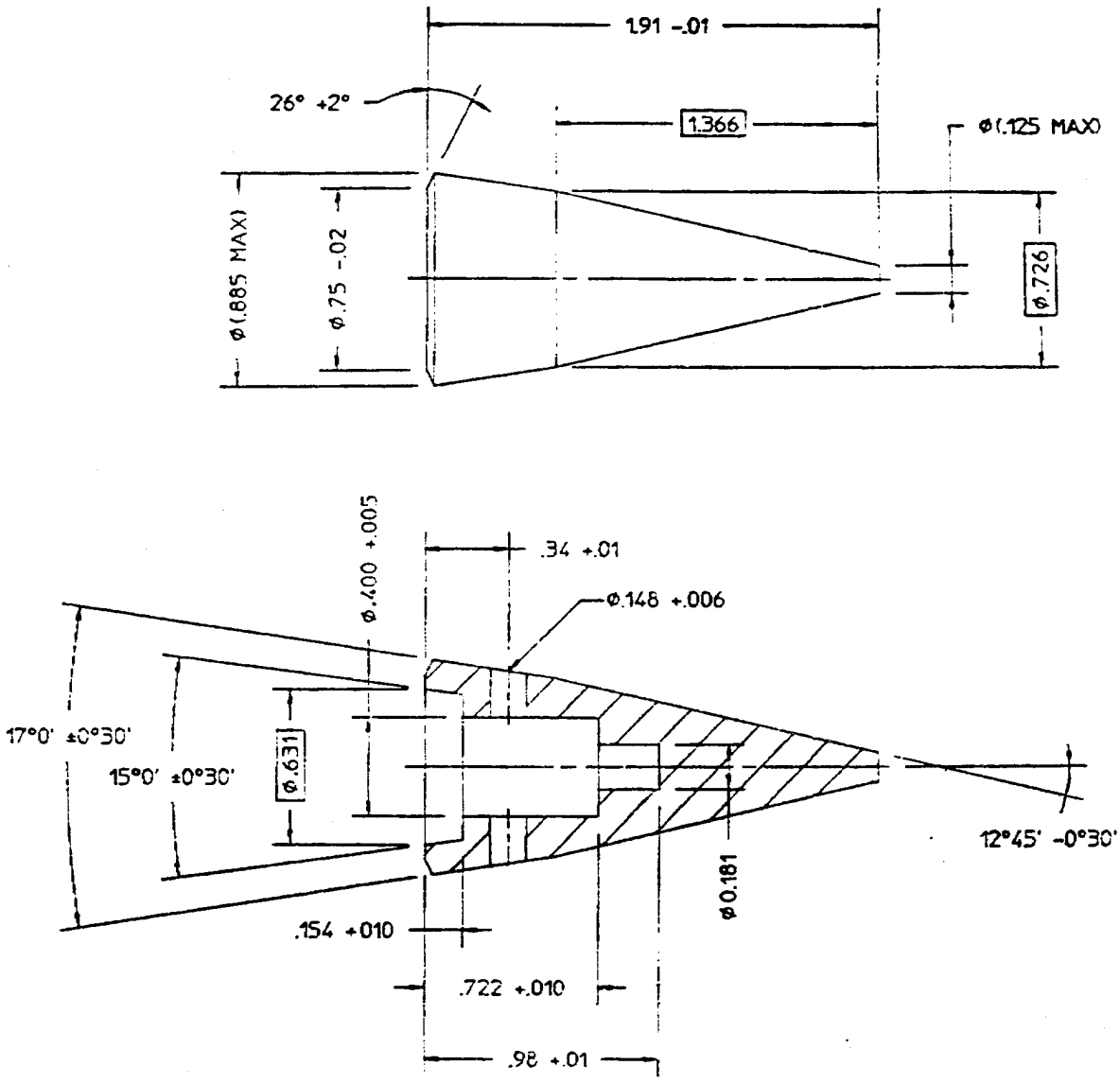

Dimensions in inches

Figure 3. Schematic of 120-mm XM797 Nosecap

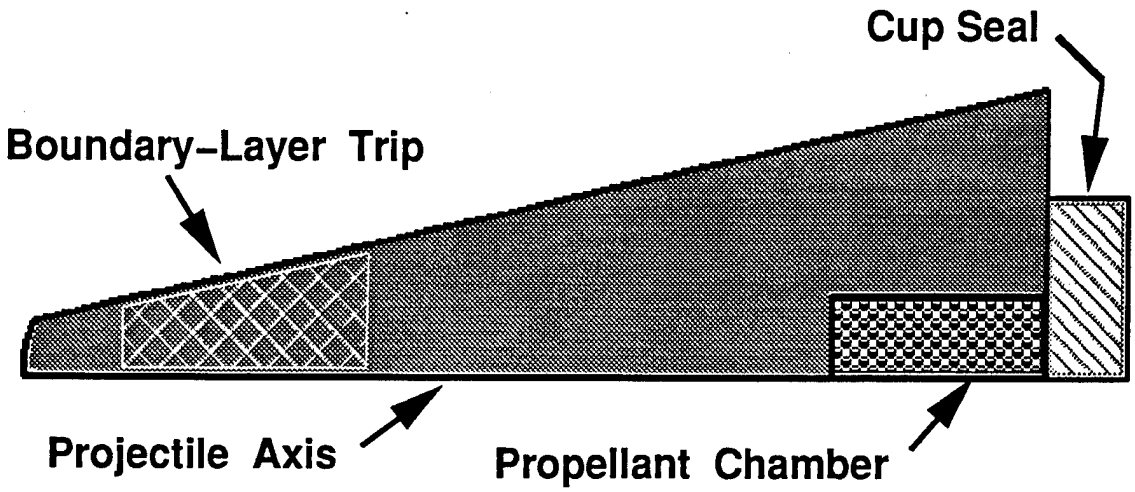

Figure 4. Heat Conduction Problem Setup

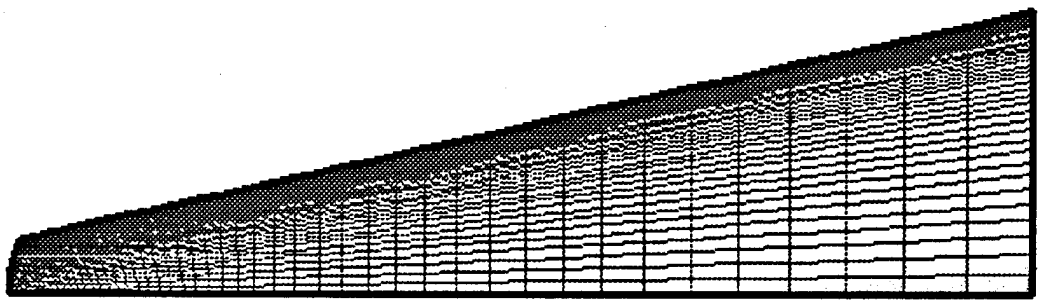

Figure 5. Single-Zone, Single-Material, Heat Conduction Grid

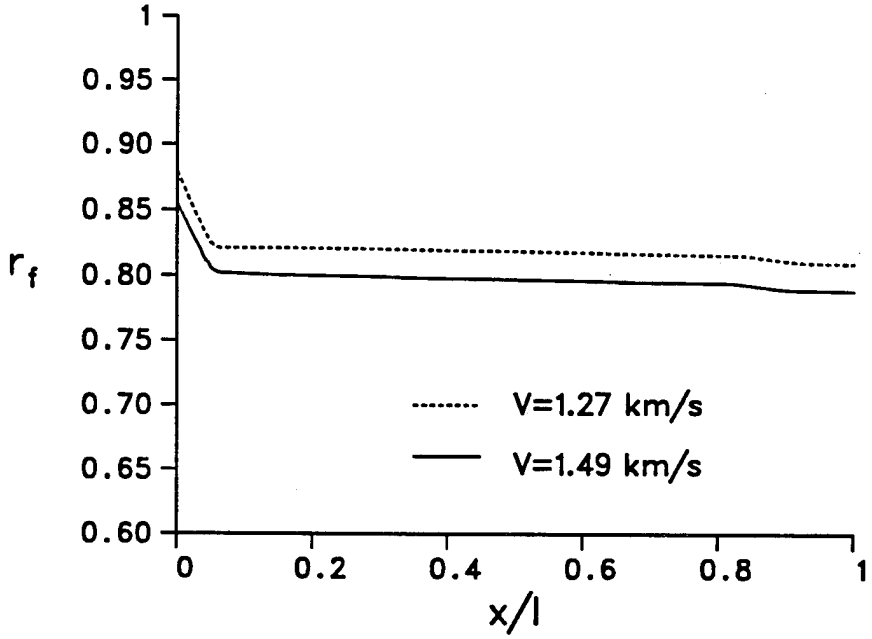

Figure 6. 105-mm XM797 Temperature Recovery Factor

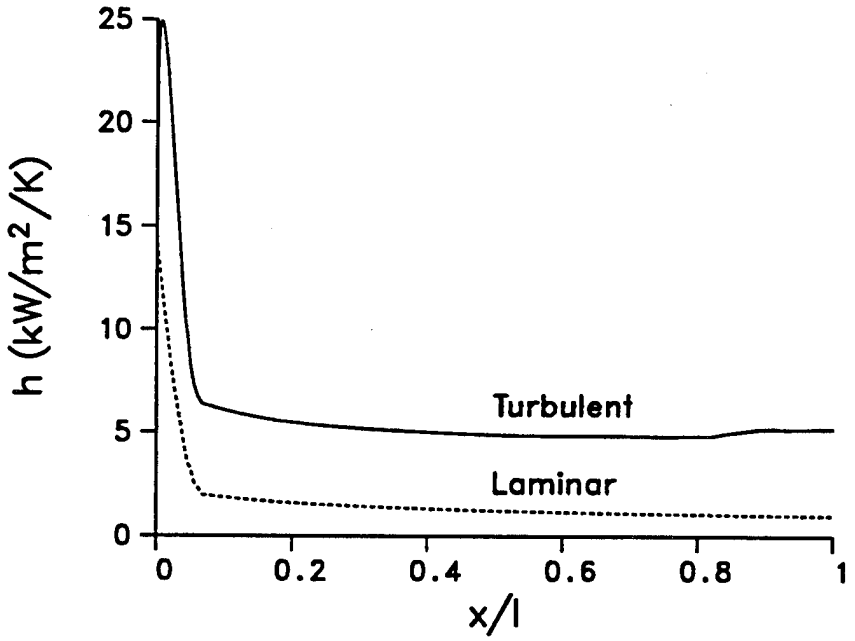

Figure 7. 105-mm XM797 Heat Transfer Coefficient, V=1.49 km/s

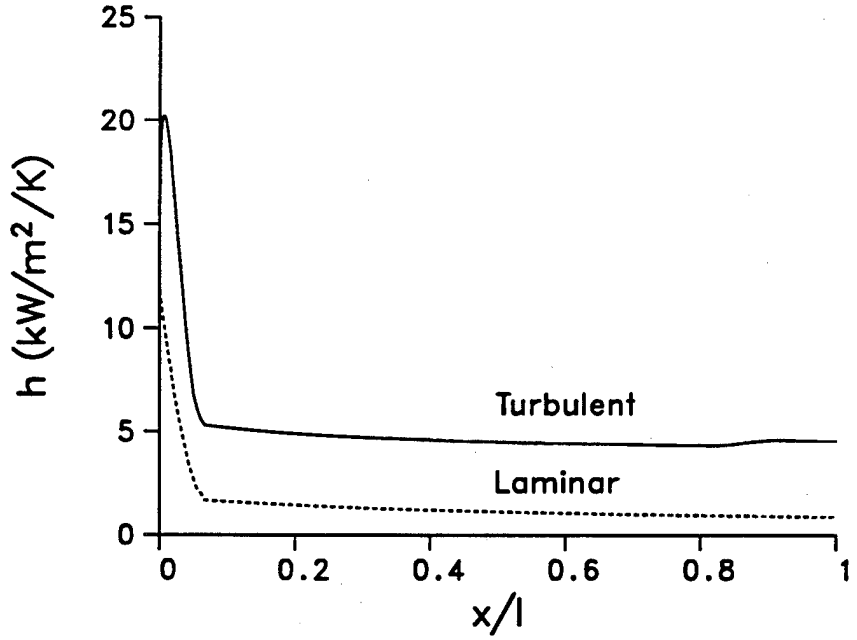

Figure 8. 105-mm XM797 Heat Transfer Coefficient, V=1.27 km/s

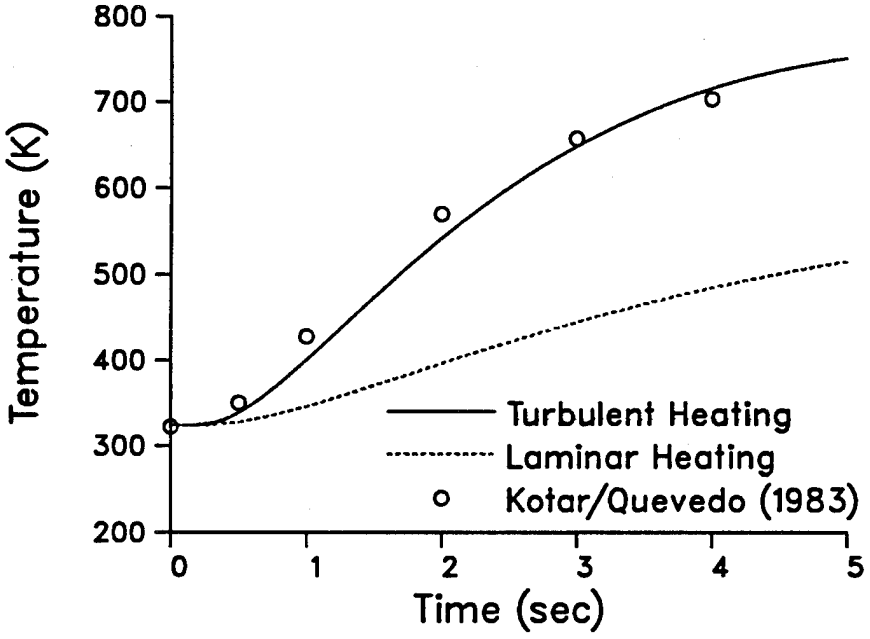

Figure 9. 105-mm XM797 Propellant Temperature Response

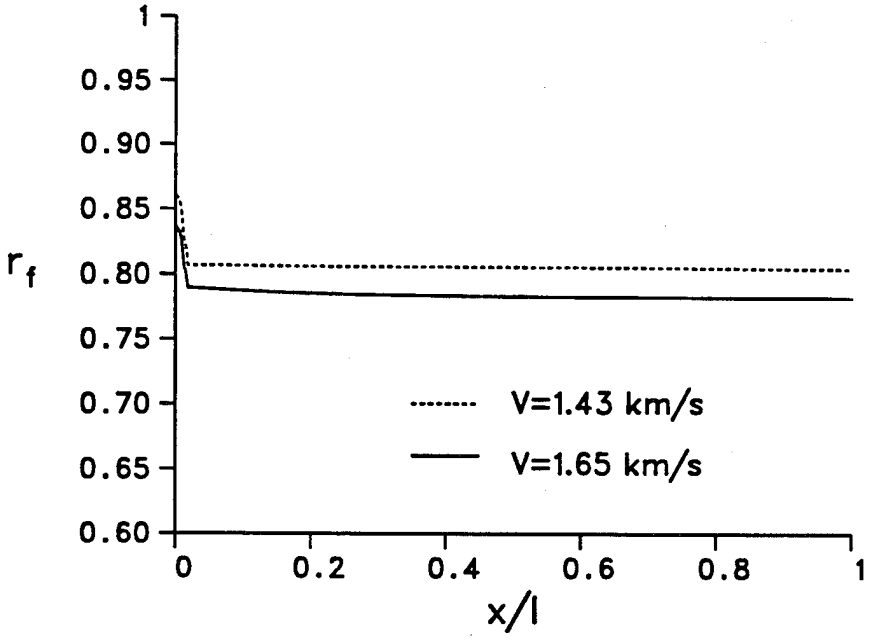

Figure 10. 120-mm XM797 Temperature Recovery Factor

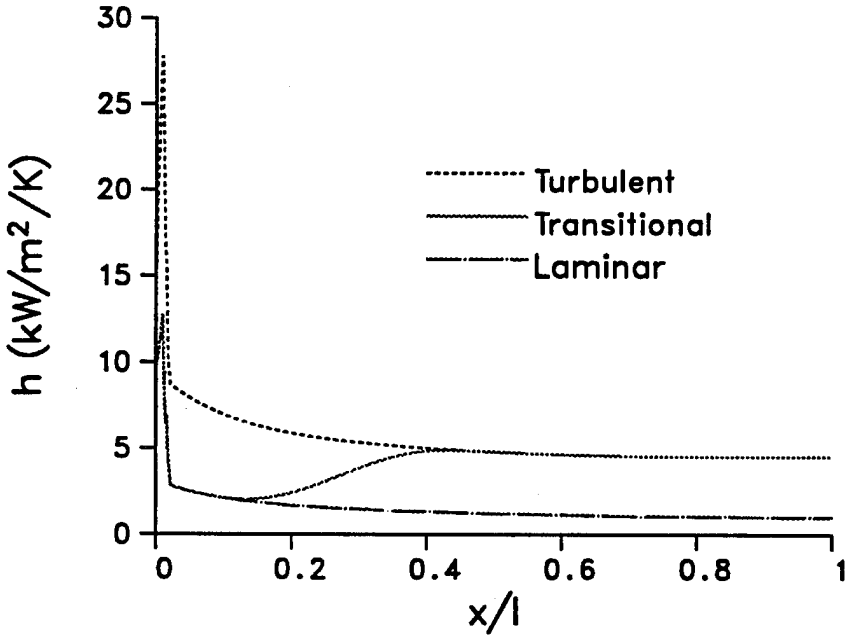

Figure 11. 120-mm XM797 Heat Transfer Coefficient, V=1.65 km/s

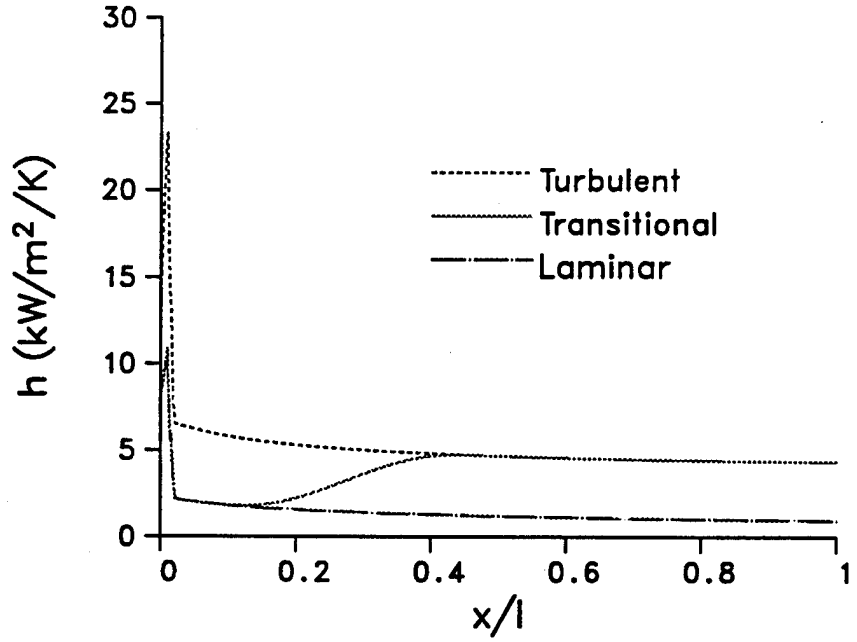

Figure 12. 120-mm XM797 Heat Transfer Coefficient, V=1.43 km/s

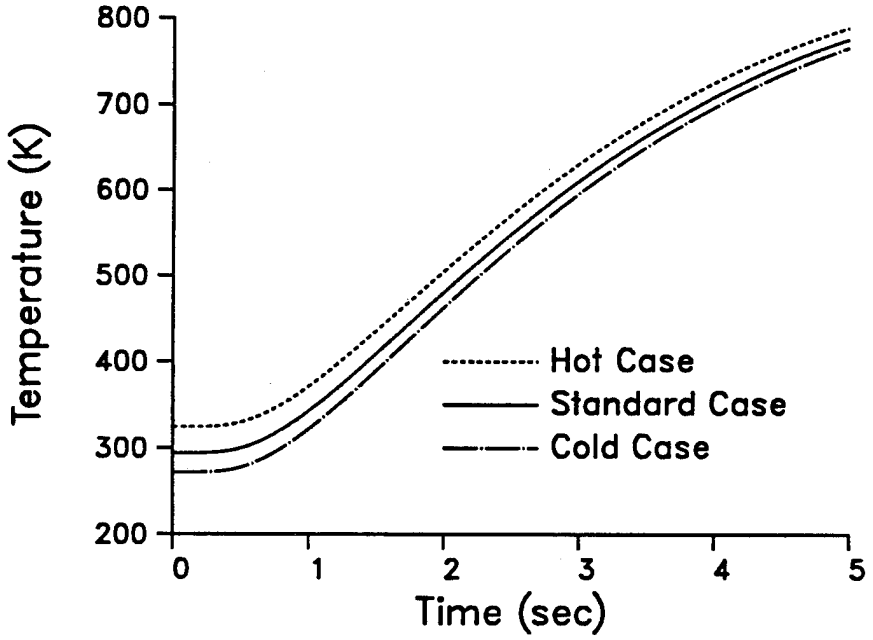

Figure 13. 120-mm XM797 Propellant Temperature Response

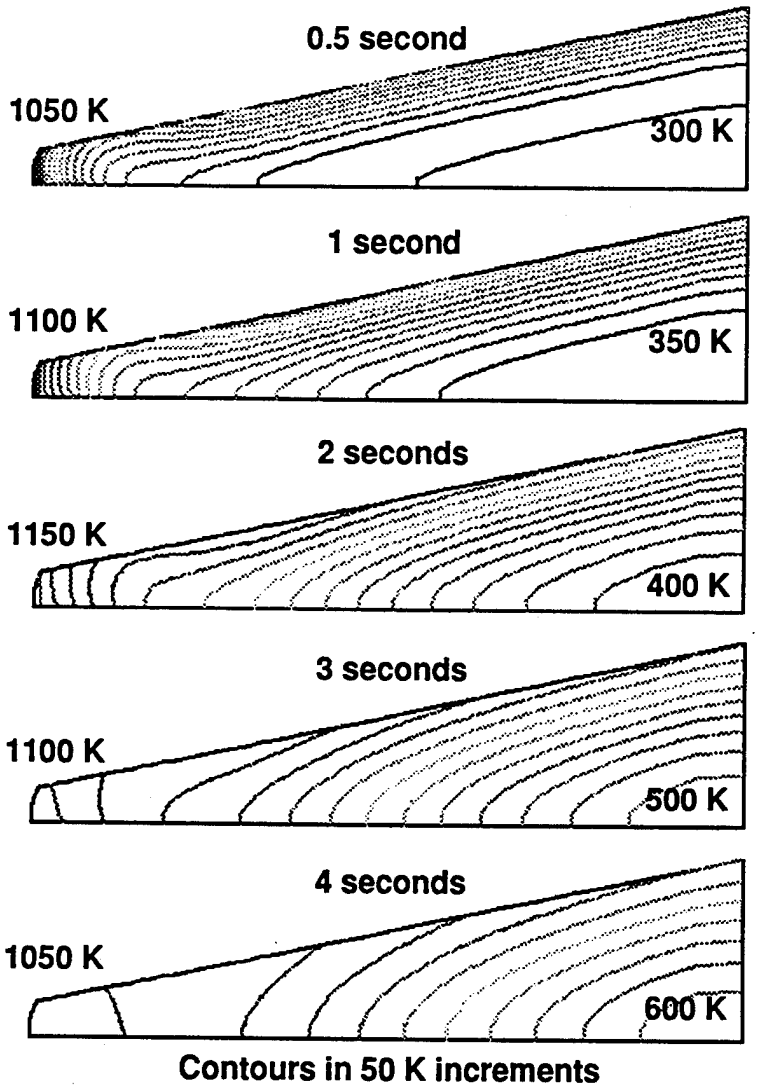

Figure 14. 120-mm XM797 Temperature Contours

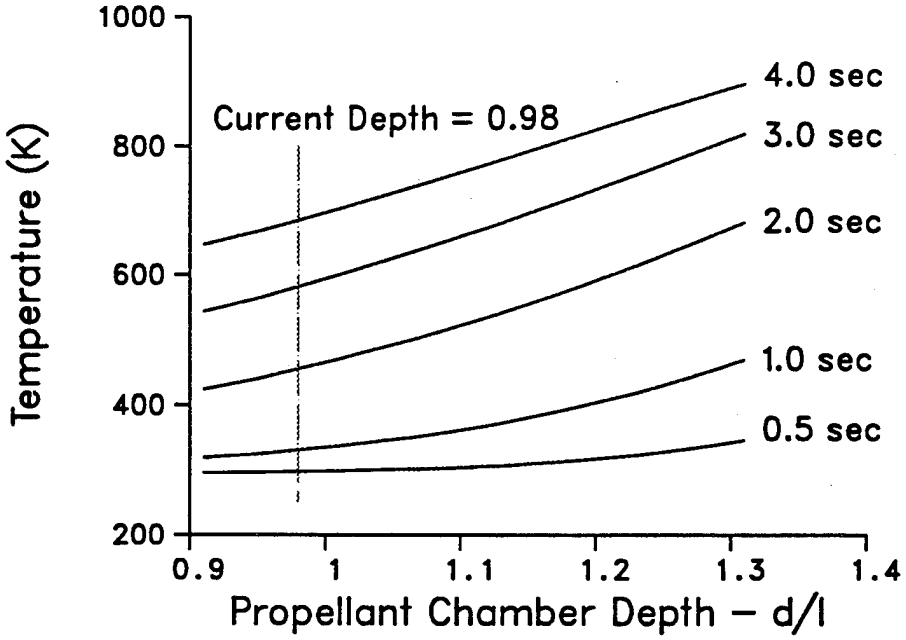

Figure 15. Effect of Chamber Depth on 120-mm XM797 Propellant Temperature Response

6. REFERENCES

Abbett, M., R. Duiven, B. Laub, and R. Beck, "Thermal and Structural Analysis of Training Round Nose Caps," U.S. Army Ballistic Research Laboratory, Aberdeen Proving Ground, Maryland, Contract Report ARBRL-CR-00455, prepared by Acurex Corporation/Aerotherm, Mountain View, California, May 1981. (AD A100712)

Cohen, A., R. Beyer, S. Bilyk, and J. Newberry, "Laser Ignition of Solid Propellants: Comparison of Model Predictions with Emission and Pressure Measurements," 29th JANNAF Combustion Subcommittee Meeting, CPIA Publication 593, Vol. 1, pp. 123, October 1992.

Product Information Chart, provided by Du Pont, Polymer Products Dept., Wilmington, Delaware, March 1995.

Dwyer, H., "Calculation of Low Mach Number Reacting Flows," AIAA Journal, Vol. 28, No. 1, pp. 98-105, January 1990.

Guidos, B., and W. Sturek, "Computation of Hypersonic Nosetip Heat Transfer Rates for an M829-Like Projectile," U.S. Army Research Laboratory, Aberdeen Proving Ground, Maryland, ARL-MR-52, April 1993. (AD 263226)

Guidos, B., and P. Weinacht, "Parabolized Navier-Stokes Computation of Surface Heat Transfer Characteristics for Supersonic and Hypersonic KE Projectiles," U.S. Army Research Laboratory, Aberdeen Proving Ground, Maryland, ARL-TR-191, August 1993. (AD A268858)

Guidos, B., P. Weinacht, and D. Dolling, "Comparison of Navier-Stokes Computation and Experiment for Pointed, Spherical, and Flat Tipped Shell at Mach 2.95," U.S. Army Research Laboratory, Aberdeen Proving Ground, Maryland, BRL-TR-3076, January 1990. (AD A218749)

Kobayashi, W., "Aerodynamic Heating Computations for Projectiles - Volume I: Indepth Heat Conduction Modifications to the ABRES Shape Change Code," U.S. Army Ballistic Research Laboratory, Aberdeen Proving Ground, Maryland, Contract Report ARBRL-CR-00527, prepared by Acurex Corporation / Aerotherm Division, Mountain View, California, June 1984. (AD A143252)

Kotar, F., and F. Quevedo, "Summary of the Development of Cartridge 105mm TPFSDS-T XM797," U.S. Army Armament Research, Development, & Engineering Center, Picatinny Arsenal, New Jersey, Internal Memorandum, September 1983. ARDEC Library Card Catalog No. C174,111.

Modern Plastics Encyclopedia, McGraw-Hill, Inc., New York, New York, Vol. 68, No. 11, p387, October 1991.

Schneider, P., Conduction Heat Transfer, Addison-Wesley Publishing Co., Inc., Cambridge, Massachusetts, 1955.

Sturek, W., "Unsteady Thermal Response to Aerodynamic Heating for Sphere-Cone and Swept-Fin Configurations at High Velocity," U.S. Army Research Laboratory, Aberdeen Proving Ground, Maryland, ARL-MR-102, August 1993. (AD B175796)

Sturek, W., H. Dwyer, and E. Ferry, Jr., "Prediction of In-Bore and Aerodynamic Heating of KE Projectile Fins," U.S. Army Ballistic Research Laboratory, Aberdeen Proving Ground, Maryland, BRL-MR-3852, August 1990. (AD A226402)

Sturek, W., L. Kayser, and D. Mylin, "Boundary-Layer Trip Effectiveness and Computations of Aerodynamic Heating for XM797 Nose-Tip Configurations," U.S. Army Ballistic Research Laboratory, Aberdeen Proving Ground, Maryland, ARBRL-MR-03262, April 1983. (AD A128036)

Sturek, W., L. Kayser, D. Mylin, and H. Hudgins, "Computational Modeling of Aerodynamic Heating for XM797 Nose Cap Configurations," U.S. Army Ballistic Research Laboratory, Aberdeen Proving Ground, Maryland, ARBRL-TR-02523, September 1983. (AD A133684)

Suchsland, K., "Aerothermal Assessment of Projectiles Using the ABRES Shape Change Code (ASCC)," Acurex Corporation / Aerotherm Division, Mountain View, California, Acurex Report TM-80-31/AS, July 1980.

Ward, J., "Specific Heat of X14 Propellant," AIAA Journal, Vol. 12, No. 1, pp. 107-108, January 1974.

Yam, C., "An Investigation of Flow Structure and Heat Transfer Characteristics of Three Dimensional Flows," PhD Dissertation in Mechanical Engineering, University of California at Davis, California, 1991.

Zucrow, M., and J. Hoffman, Gas Dynamics, Volume I, John Wiley & Sons, New York, 1976.

APPENDIX:
1-D AXISYMMETRIC HEAT CONDUCTION VALIDATION

INTENTIONALLY LEFT BLANK.

This appendix presents comparisons between numerical and analytical results for a 1-D axisymmetric heat conduction problem. The heat conduction code described in the main body of this report was used to obtain the numerical result. The configuration is an infinite length steel cylinder subjected to axisymmetric convective heating, in which the heat transfer coefficient, h, is held constant. The problem inputs somewhat typify the length scale and heating environment that could be experienced by a projectile in supersonic/hypersonic flight. Table A-1 shows the material properties of the cylinder, as well as the initial and boundary conditions.

Table A-1. 1-D Axisymmetric Heat Conduction Validation Problem Conditions

Material: Mild Steel	
Density, ρ (kg/m^3)	7850.0
Conductivity, k (W/m/K)	45.3
Specific Heat c_p (J/kg/K)	444.6
Diffusivity, $\alpha=\frac{k}{\rho c_p}$ (m^2/s)	1.3×10^{-5}
Cylinder Radius, r_0 (m)	.0127
Initial Temperature, T_i (K)	294.
Adiabatic Wall Temperature, T_{aw} (K)	1800.
Heat Transfer Coefficient, h (W/m^2/K)	5000.
Nusselt Number, $N_u = \frac{hr_0}{k}$	1.4

The governing equation is

$$\frac{\partial^2 T}{\partial r^2} + \frac{1}{r}\frac{\partial T}{\partial r} = \frac{1}{\alpha}\frac{\partial T}{\partial t} \tag{A-1}$$

An analytical solution is described by Schneider.[1] The temperature, T, is a function of radial location, r, and time, t, and is given by

$$T = T_{aw} + 2(T_i - T_{aw}) \sum_{n=1}^{\infty} \frac{1}{M_n} \frac{J_1(M_n)}{J_0^2(M_n) + J_1^2(M_n)} e^{-M_n^2 \Theta} J_0(M_n \frac{r}{r_0}) \tag{A-2}$$

In the above expression, J_0 and J_1 are Bessel functions of order zero and one, respectively. The variable Θ is defined as

$$\Theta = \frac{\alpha t}{r_0^2} \tag{A-3}$$

The variable M_n is the nth root of the eigenfunction Bessel equation

$$M \frac{J_1(M)}{J_0(M)} = N_u \tag{A-4}$$

[1] Schneider, P., Conduction Heat Transfer, Addison-Wesley Publishing Co., Inc., Cambridge, Massachusetts, 1955.

This equation has an infinite number of roots, which are found using Newton's method. The equation is first arranged to comprise the function f:

$$f(M) = M\frac{J_1(M)}{J_0(M)} - N_u \tag{A-5}$$

The derivative of f is

$$f'(M) = \frac{M[J_0^2(M) + J_1^2(M)]}{J_0} \tag{A-6}$$

and the iteration to convergence is performed using the algorithm

$$M_n^{i+1} = M_n^i - \frac{f(M_n^i)}{f'(M_n^i)} \tag{A-7}$$

in which the superscript i refers to the iteration number for any particular root that is being sought. The initial value for the nth root, constructed here based on the table provided by Schneider for the eigenfunction Bessel equation and the known value of N_u, is

$$\begin{aligned} M_n^1 &= 1.4 && \text{for} \quad n = 1 \\ M_n^1 &= 4.6 + (n-2)\pi && \text{for} \quad n = 2, 3, 4, \ldots \end{aligned} \tag{A-8}$$

The analytical results presented here were generated using the first 40 terms from Equation (A-2), corresponding to the first 40 roots of the eigenfunction Bessel equation. Forty terms provided accuracy to at least four decimal places.

Figure A-1 shows the temperature response of the cylinder axis ($r/r_0 = 0$) and surface ($r/r_0 = 1$) as a function of time. The analytical and numerical results are both shown and are virtually indistinguishable. The largest observable difference between the numerical and analytical results occurs on the axis at approximately 1 second. A closer examination is made in Figure A-2, which shows the numerical and analytical temperature distributions in the cylindrical rod at $t = 0.9627$ seconds. The agreement on the axis is within 7 K, and the agreement elsewhere is mostly within 1 to 2 K. The disageement near the cylinder axis, which is acceptable for the engineering application in this report, is attributable to the combination of large grid cells near the axis and the first order axis boundary condition in the numerical code.

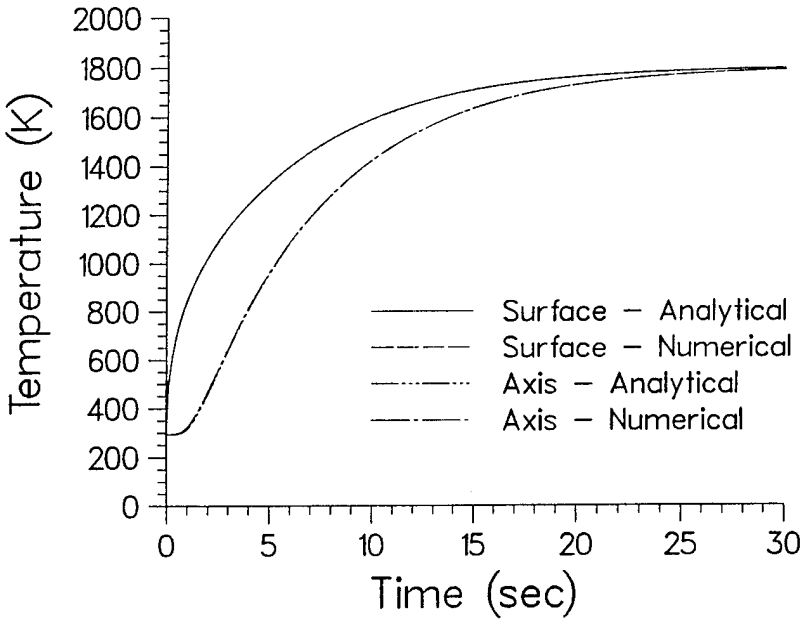

Figure A-1. 1-D Axisymmetric Heat Conduction Validation: Temperature vs. Time

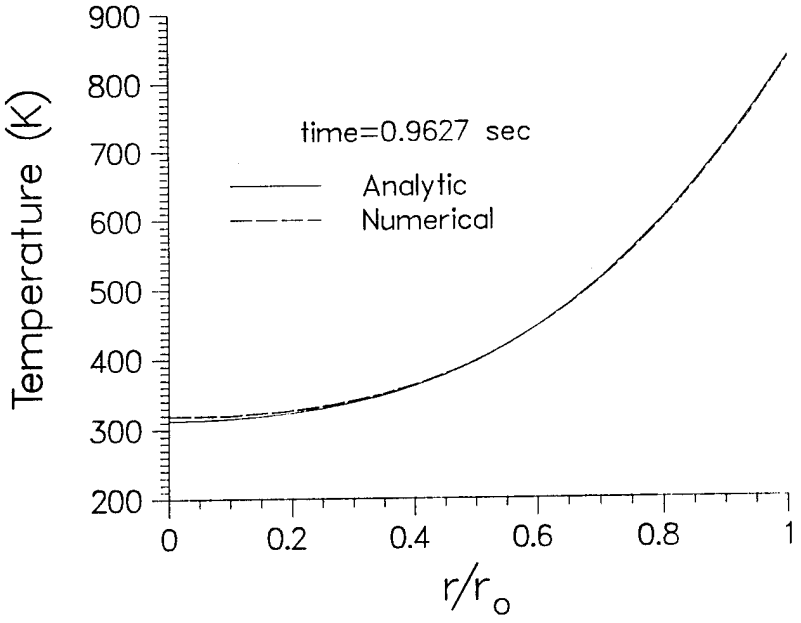

Figure A-2. 1-D Axisymmetric Heat Conduction Validation: Temperature vs. Location

INTENTIONALLY LEFT BLANK.

LIST OF SYMBOLS

c_p	specific heat
d	propellant chamber depth
h	surface heat transfer coefficient
J_n	Bessel function of order n
k	thermal conductivity
l	reference length, equal to 25.4 mm (1 inch)
M_n	nth root of eigenfunction Bessel equation
N_u	Nusselt number
q	surface heat transfer rate
r	radial distance from x-axis
r_0	radius of infinite length cylinder
r_f	surface temperature recovery factor
T	temperature
t	time
V	projectile velocity
x	distance along projectile axis, measured from nosetip

Greek Symbols

α	thermal diffusivity
κ_t	boundary layer transition intermittency factor
ρ	density

Subscript

∞	free stream condition
aw	adiabatic wall condition
i	initial condition
l	laminar boundary layer flow condition
0	total condition
t	turbulent boundary layer flow condition
tr	transitional boundary layer flow condition
w	wall condition

INTENTIONALLY LEFT BLANK.

NO. OF
COPIES ORGANIZATION

2 ADMINISTRATOR
DEFENSE TECHNICAL INFO CTR
ATTN DTIC DDA
CAMERON STATION
ALEXANDRIA VA 22304-6145

1 DIRECTOR
US ARMY RESEARCH LAB
ATTN AMSRL OP SD TA
2800 POWDER MILL RD
ADELPHI MD 20783-1145

3 DIRECTOR
US ARMY RESEARCH LAB
ATTN AMSRL OP SD TL
2800 POWDER MILL RD
ADELPHI MD 20783-1145

3 DIRECTOR
US ARMY RESEARCH LAB
ATTN AMSRL OP SD TP
2800 POWDER MILL RD
ADELPHI MD 20783-1145

ABERDEEN PROVING GROUND

5 DIR USARL
ATTN AMSRL OP AP L (305)

NO. OF
COPIES ORGANIZATION

6 COMMANDER
US ARMY ARMAMENT RD&E CTR
ATTN AMSTA AR AET A
M AMORUSO
S CHUNG
S KAHN
C LIVECCHIA
C NG
B WONG
PICATINNY ARSENAL NJ 07806-5000

5 COMMANDER
US ARMY ARMAMENT RD&E CTR
ATTN AMSTA AR CCH B
E FENNELL
T LOUZEIRO
D KITCHEN
B KONRAD
F QUEVEDO
PICATINNY ARSENAL NJ 07806-5000

5 COMMANDER
US ARMY ARMAMENT RD&E CTR
ATTN AMSTA AR FSE
E ANDRICOPOULIS
K CHEUNG
A GRAF
D LADD
PICATINNY ARSENAL NJ 07806-5000

6 COMMANDER
US ARMY ARMAMENT RD&E CTR
ATTN AMSTA AR CCL B
D CONWAY
D DAVIS
K HAYES
M PINCAY
F PUZYCKI
W SCHUPP
PICATINNY ARSENAL NJ 07806-5000

2 COMMANDER
US ARMY ARMAMENT RD&E CTR
ATTN AMSTA AR CCH A
J DIFUCCI
M PALATHINGAL
PICATINNY ARSENAL NJ 07806-5000

NO. OF
COPIES ORGANIZATION

3 U.S. ARMY RESEARCH OFFICE
ATTN G ANDERSON
K CLARK
T DOLIGOWSKI
PO BOX 12211
RESEARCH TRIANGLE PARK NC 27709-2211

2 DIRECTOR
US ARMY BENET LABORATORY
ATTN SMCAR CCB R
P AALTO
S SOPOK
WATERVALIET NY 12189

1 DIRECTOR
US BELVOIR RD&E CTR
ATTN SATBE FED
N BLACKWELL
FORT BELVOIR VA 22060-5606

2 COMMANDER
UNITED STATES MILITARY ACADEMY
DEPARTMENT OF CIVIL
AND MECHANICAL ENGINEERING
ATTN M COSTELLO
A DULL
WEST POINT NY 10996

4 HERCULES INC
ALLEGANY BALLISTICS LABORATORY
ATTN J CONDON
W NYGA
J PARRILL
J VILES
PO BOX 210
ROCKET CTR WV 26726

NO. OF COPIES ORGANIZATION

ABERDEEN PROVING GROUND

5 COMMANDER
US ARMY ARMAMENT RD&E CTR
ATTN AMSTA AR FSF T
S LIESKE
J MATTS
F MIRABELLE
S PUHALLA
J WHITESIDE

41 DIRECTOR
US ARMY RESEARCH LABORATORY
ATTN AMSRL SC CC
R ANGELINI
C NIETUBICZ
J GROSH
D HISLEY
AMSRL SC I W STUREK
AMSRL WT P
A HORST
E SCHMIDT
AMSRL WT PA
P CONROY
G KELLER
D KRUCZYNSKI
T MINOR
M NUSCA
AMSRL WT PB
H EDGE
J GARNER
B GUIDOS (5)
K HEAVEY
P PLOSTINS
J SAHU
P WEINACHT
AMSRL WT PC
G ADAMS
R FIFER
AMSRL WT PD
B BURNS
W DRYSDALE
R LIEB
S WILKERSON
AMSRL WT W
C MURPHY
AMSRL WT WB
F BRANDON
T BROWN
W D'AMICO
D HEPNER
M HOLLIS
AMSRL WT WC
J BORNSTEIN
R VON WAHLDE

NO. OF COPIES ORGANIZATION

AMSRL WT WD
T KOTTKE
C STUMPFEL
AMSRL WT NC
R LOTTERO
S SHRAML

INTENTIONALLY LEFT BLANK.

USER EVALUATION SHEET/CHANGE OF ADDRESS

This Laboratory undertakes a continuing effort to improve the quality of the reports it publishes. Your comments/answers to the items/questions below will aid us in our efforts.

1. ARL Report Number ARL-MR-267 Date of Report October 1995

2. Date Report Received _____

3. Does this report satisfy a need? (Comment on purpose, related project, or other area of interest for which the report will be used.) _____

4. Specifically, how is the report being used? (Information source, design data, procedure, source of ideas, etc.) _____

5. Has the information in this report led to any quantitative savings as far as man-hours or dollars saved, operating costs avoided, or efficiencies achieved, etc? If so, please elaborate. _____

6. General Comments. What do you think should be changed to improve future reports? (Indicate changes to organization, technical content, format, etc.) _____

CURRENT ADDRESS

_____
Organization

_____
Name

_____
Street or P.O. Box No.

_____
City, State, Zip Code

7. If indicating a Change of Address or Address Correction, please provide the Current or Correct address above and the Old or Incorrect address below.

OLD ADDRESS

_____
Organization

_____
Name

_____
Street or P.O. Box No.

_____
City, State, Zip Code

(Remove this sheet, fold as indicated, tape closed, and mail.)
(DO NOT STAPLE)